RSC Publishing Faraday Discussions

Low-Current Field-Assisted Assembly of Copper Nanoparticles for Current Collectors

Journal:	*Faraday Discussions*
Manuscript ID:	FD-ART-12-2014-000263.R1
Article Type:	Paper
Date Submitted by the Author:	04-Feb-2015

Complete List of Authors:	Kotov, Nicholas; University of Michigan, Department of Chemical Engineering liu, Lehao; University of Michigan, Chemical Engineering Choi, Bong; National Nanofab Center, Center for Nanobio Integration & Convergence Engineering Tung, Siu; University of Michigan, Chemical Engineering Hu, Tao; Harbin Institute of Technology, Key Laboratory of Microsystems and Micronanostructures Manufacturing, Ministry of Education Liu, Yajie; University of Michigan, Chemical Engineering Li, Tiehu; Northwestern Polytechnical University, School of Materials Science and Engineering Zhao, Tingkai; Northwestern Polytechnical University,

Low-Current Field-Assisted Assembly of Copper Nanoparticles for Current Collectors

Lehao Liu[†,‡], Bong Gill Choi[‡], Siu On Tung[§], Tao Hu[‡], Yajie Liu[‡], Tiehu Li[†], Tingkai Zhao[†], and Nicholas A. Kotov[‡,⊥,*]

[†]School of Materials Science and Engineering, Northwestern Polytechnical University, Xi'an 710072, Shaanxi, P. R. China; [‡]Department of Chemical Engineering, University of Michigan, Ann Arbor, Michigan 48109, USA; [§]Macromolecular Science and Engineering, University of Michigan, Ann Arbor, Michigan 48109, USA; [⊥]Biointerfaces Institute, University of Michigan, Ann Arbor, Michigan 48109, USA.

*To whom correspondence should be addressed: kotov@umich.edu.

ABSTRACT: Current collectors are essential parts of batteries and many other electronic devices. They are responsible for efficient charge transport to active electrode materials. Three-dimensional (3D) high surface area current collectors considerably improve performance of cathodes and anodes in batteries, but their technological implementation is impeded by the complexity of their preparation, which needs to be simple, fast, and energy efficient. Here we demonstrate that field-stimulated assembly of ~3 nm copper nanoparticles (NPs) enables the preparation of porous Cu NP films. The use of NP dispersions enables 30x reduction of the deposition current for making functional 3D coatings. In addition to high surface area, lattice-to-lattice connectivity in self-assembly of NP in 3D structures enables fast charge transport. The mesoscale dimensions of out-of-plane features and spacing between them in Cu films made by field-stimulated self-assembly of NPs provides promising morphology for current collection in lithium ion batteries (LIBs). Half-cells electrochemical models based on field-stimulated self-assembled films show improved specific capacity, total capacity, and cycle performance compared to traditional flat and other 3D current collectors. While integration of active electrode material into the 3D topography of the current collector needs to be improved, this study indicates that self-assembled NP films represent a viable manufacturing approach for 3D electrodes.

KEYWORDS: copper nanoparticles • current collector • porous copper nanoparticle films • electro-deposition • three-dimensional electrodes • graphite • lithium ion batteries • metallic coatings

1. INTRODUCTION

Lithium ion batteries (LIBs) are widely used as a versatile power source and represent one of the central elements of green energy technologies. However, increasing energy/power densities and charge-discharge (C-D) rates required for electrical vehicles, smart electrical grid systems, wearable electronic devices, etc remains a considerable technological challenge.[1-2] It necessitates innovation in all components of LIB and other batteries. Current collectors are essential element of all batteries and many other electronic devices. They serve as an interface between leads and the active electrode materials and have particular importance for new generation of LIBs. Current collectors are usually made of foils from stainless steel, nickel, copper, carbon materials, or aluminum. The relatively smooth surface of these foils simplifies the manufacturing process but is, in fact, not the best for the performance of the batteries and other devices. The "flatness" (in the context of this study this term indicates the lack of specific meso- a microscale protrusions on the surface of the electrode) of traditional current collectors reduces the contact area available for (1) electron transfer with and (2) adhesion of anode/cathode materials to the electrodes.[3-6] The physical and chemical changes occurring with anode/cathode during the lithiation-delithiation process exacerbates this problem. "Flatness" of current collectors facilitate delamination of active materials from the electrodes which is a serious challenge for both high discharge rate batteries and flexible devices suffering from thecapacity loss upon C-D cycling and flexural deformation.[4,7-11]

Porous copper,[12-13] nickel foam,[14] graphene 3D networks,[15] and carbon

paper,[10,16-17] have been studied as three-dimensional (3D) current collectors for LIBs.[18-19] Indeed, these 'sculpted' current collectors improve adhesion of active material,[4,20] and accommodate strain occurring lithiation-delithiation reaction.[12,21-22] 3D current collectors also accelerate surface electrochemical reactions[23-24] and lithium ion transport.[23] For example, a nickel foam current collector was shown to improve the C-D performance of lithium-air batteries by facilitating gas transport.[25-26] Porous copper is particularly interesting in this respect, due to its relatively low cost and mechanical/electrical properties convenient for high currents.[27-29] Copper current collectors are also well-known for their chemical compatibility with battery electrolytes and ability for improving cycle performance of LIBs.[30-32]

The methods for preparing of porous copper and other 3D metallic films include casting,[33-34] powder metallurgy,[35] electro-deposition,[36-38] and dealloying,[39-40] while the preparation of carbon-based current collectors is typically done using sacrificial templates.[15] Although these methods can be powerful research tools for constructing materials with promising performance, their successful implementation in actual LIBs has been impeded by multiple problems originating from the complexity of the preparative process. These problems include high energy/time requirements,[39-40] incompatible pore sizes and thicknesses,[4] environmental concerns,[36-38] reduced load of the active material,[41] and difficulties of integration with anode and cathode materials.[21,42]

In this study, we developed a method for the preparation of a porous Cu film based on the field-stimulated assembly of copper nanoparticles (Cu NPs) that can

alleviate some of these problems. This method utilizes intrinsic ability of NPs to produce complex 3D structures with nano- and microscale surface topology rather than relying on sacrificial templates. Field-stimulated assembly is simple, fast and requires less energy than other methods of the preparation of 3D current collectors. As such, the time requirements are reduced by at least an order of magnitude compared to calcination processes.[43-46] Furthermore, the electrical current in our process is reduced by an at least an order of magnitude compared to electro-deposition processes. From the materials engineering perspective, it is also significant that the field-assisted assembly of NPs affords lattice-to-lattice connectivity between NPs in the 3D network leading to efficient charge transport throughout the film. We demonstrated that current collectors obtained by this method can successfully serve in LIBs in conjunction with traditional dispersion-processed carbon (theoretical capacity: 372 mAh g^{-1}).[47-48] They demonstrated improved the capacity and cycling performance compared to Cu foils and other porous Cu electrodes.[41]

2. RESULTS AND DISCUSSION

2.1. Starting dispersions of Cu NPs. One of the most essential steps in the successful assembly is the selection of suitable NPs as "building blocks". One of the primary requirements to the building block of the potential current collector was that the colloidal stability of NPs must not compromise the conductivity in the assembled structure. Reaching high mobility of charge carriers in thin films of NPs is known to be challenging even for metal NPs because the presence of organic coating on the

surface of NPs stabilizing NPs in dispersions creates high tunneling barrier.[49] Previous efforts of incorporation of water-soluble NPs in electronic devices indicated that spontaneous removal of the coating and efficient transport from NP to NP is possible.[50] Also, the use of thin citrate-based coatings was shown to drastically facilitate the charge transport between the NPs of gold.[51] But the current collectors are unlikely to be made from gold (unless for some high value implantable biomedical devices) and citrate stabilization of Cu NPs was accompanied with formation an oxidation layer.

Finding a suitable NP dispersion for this project was challenging because of high requirements to electronic conductivity in current collectors. Considerations of the materials cost and most common metal used for current collectors led us to Cu NP. Previous studies demonstrated, however, that while being technologically attractive, Cu NP dispersions and inks present considerable chemical challenges.[52-55] Besides the fundamental stability-conductivity dilemma,[49] the dispersions of Cu NPs are prone to more extensive agglomeration than NPs from other metals, for instance well-known gold nanocolloids, due to lower surface charge.[52-53,56] Also, Cu NPs are more chemically active than gold or silver NPs, which makes them susceptible to oxidation,[52,57-58] especially in aqueous media.[54,59] Protection from oxidation and colloidal stabilization required thick organic or silica coatings on each NP,[52,60-61] which certainly prohibits their use of assembled structures from them as current collectors as well as other charge elements of electronic devices.

We decided to start this project with finding a suitable method to synthesize Cu

NPs that would be able to address these challenges. Summarizing the requirements for synthetic recipe, the Cu NP dispersions need to be (a) colloidally stable within the time-frame adequate for the preparation of current collectors, (b) resilient against oxidation, and (c) capable of self-assembly. An additional requirement was also that the dispersion media would be aqueous. The preference for water-based dispersions originates from the convenience, safety, and efficiency of electro-deposition in aqueous electrolytes.

The synthetic recipe satisfying all these requirements was found and described in details in Methods. In brief, an aqueous Cu NP dispersion (**Figure 1A**) was made by heating a solution of 0.03 M copper chloride in presence of 0.4 M *L*-ascorbic acid, and 0.01 M cetyltrimethylammonium bromide (CTAB) solution at 45 ^{o}C for 42 hours under vigorous stirring. The combination of CTAB provides high charge, while *L*-ascorbic acid prevents the formation of copper oxides being a mild reducing agent. Although the hydrocarbon chain in CTAB is quite long and can completely hinder interparticle electron transport, it is also known to be labile surface ligand that we took advantage in the self-assembly process.

The as-synthesized Cu NP aqueous dispersion was red, and displayed no indication of sedimentation or oxidation after one month of storage under ambient conditions (**Figure 1A**). TEM images of the dispersion displayed discrete Cu NPs with a relatively narrow size distribution (**Figure 1B and Figure S1A**). An average TEM diameter was found to be of 3.2 ± 0.74 nm by counting 754 particles (**Figure 1C**). Dynamic light scattering (DLS) of the same NP dispersions yielded an average

diameter of 10.6 nm (**Figure S1B**). The increase of apparent NP diameter in DLS data compared to TEM data was attributed to the presence of a layer from tightly bound water molecules and CTAB.

High resolution TEM revealed that the lattice spacing of the NPs is 0.21 nm (inset of **Figure 1B**); it corresponds very well to the spacing of (111) lattice planes in the face-centered cubic (FCC) Cu. The selected area electron diffraction (SAED) pattern revealed that the first, second, third and fourth diffraction rings (from center to outside) correspond to the crystal spacing of 0.21, 0.18, 0.13 and 0.11 nm, respectively. This sequence is consistent with the crystal planes of (111), (200), (220), and (311) metallic FCC Cu. Cumulatively these findings confirmed that that the prepared NPs were made from metallic Cu rather than from copper oxide(s) (**Figure 1D**).

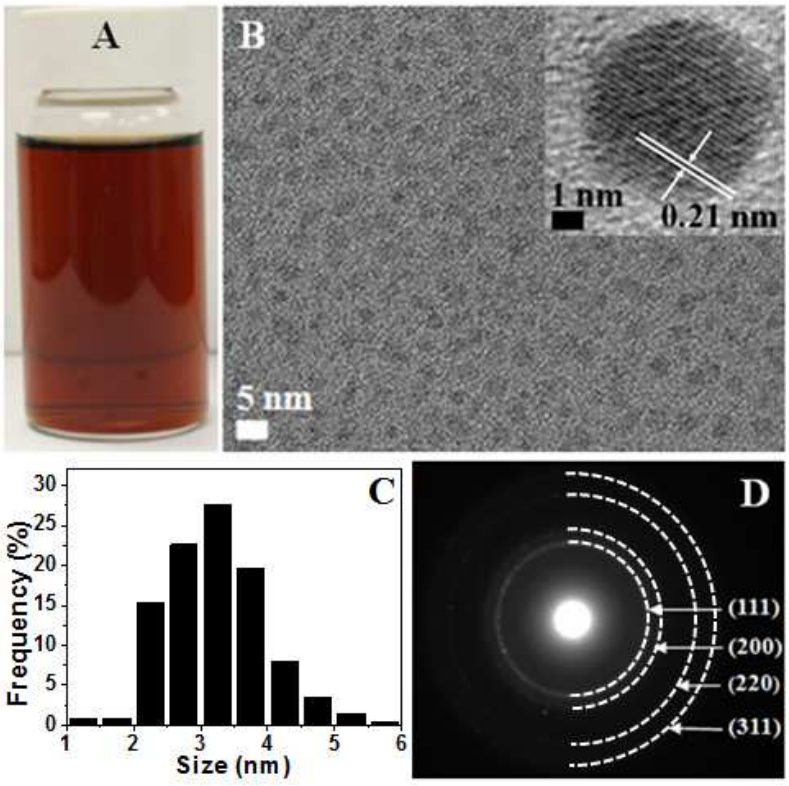

Figure 1. (A) Photograph of aqueous dispersion of prepared Cu NP after one month of storage, and (B) TEM image of Cu NPs, (C) size histogram obtained by counting Cu NPs in TEM image, and (D) the corresponding SAED pattern of Cu NPs. Inset of Figure 1 (B) shows the HR-TEM image of a Cu NP.

2.2. Field-stimulated assembly of Cu NPs into conductive films. We made porous Cu films potentially suitable to serve as 3D current collectors using two different methods: conventional electro-deposition of Cu^{2+} ions and field-stimulated assembly of Cu NPs. In both cases the Cu layer was deposited on traditional Cu foils. Surface topography of the nanoscale Cu coatings on the electrodes had distinct three-dimensionality as opposed to the starting "flat" electrodes with much less pronounced out-of-plane features (**Figure S2)**.

Electrochemical reduction of Cu^{2+} under a potential of 800 mV resulted in a macroporous Cu film (**Figure 2A-C**) with an average thickness of ~55 μm (**Figure**

2D-F). The current required to obtain such films in 8 min was ~2.4 A. The interconnected cavities on the surface of the deposited Cu had an average size of ~ 100 μm with wall thicknesses of ~10 μm, which is in agreement with previous studies.[22-23,36] The pore walls were made of dendritic Cu agglomerates with the crystal grains of several hundred nanometers in diameter; the branches were several micrometers in length. Note that the pore size is ~100 μm, which is likely to be too large for efficient current collectors.[4,41]

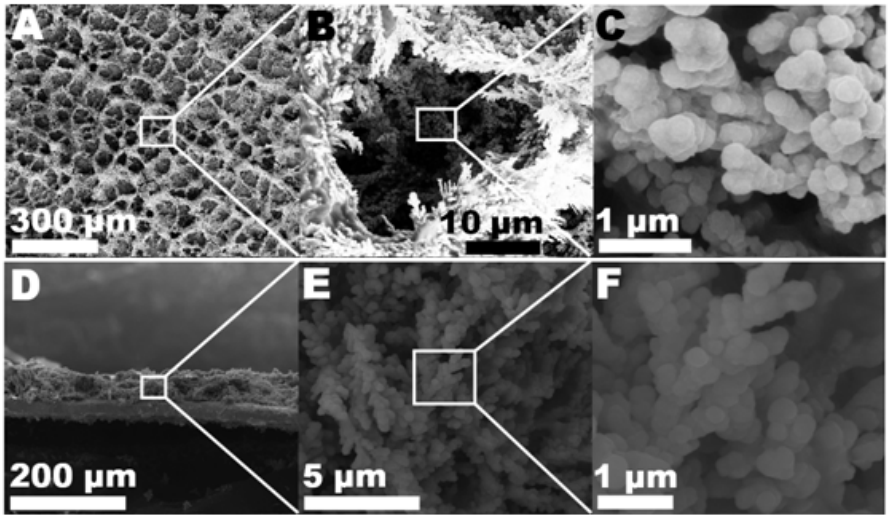

Figure 2. (A-C) Top-view and (D-F) cross-sectional SEM images of 3D Cu film by electrochemical reduction of Cu^{2+} under a potential of 800 mV for 8 min; average current ~2.4 A.

Variation of potential and reaction time of the field-stimulated assembly afforded modulation of cavity/pore sizes in Cu electrodes (**Figure 3**). As such we were able to change the pore size from 50 to 200 nm. According to the previous studies,[4,13,41] these dimensions are suitable for efficient charge extraction from electroactive materials.

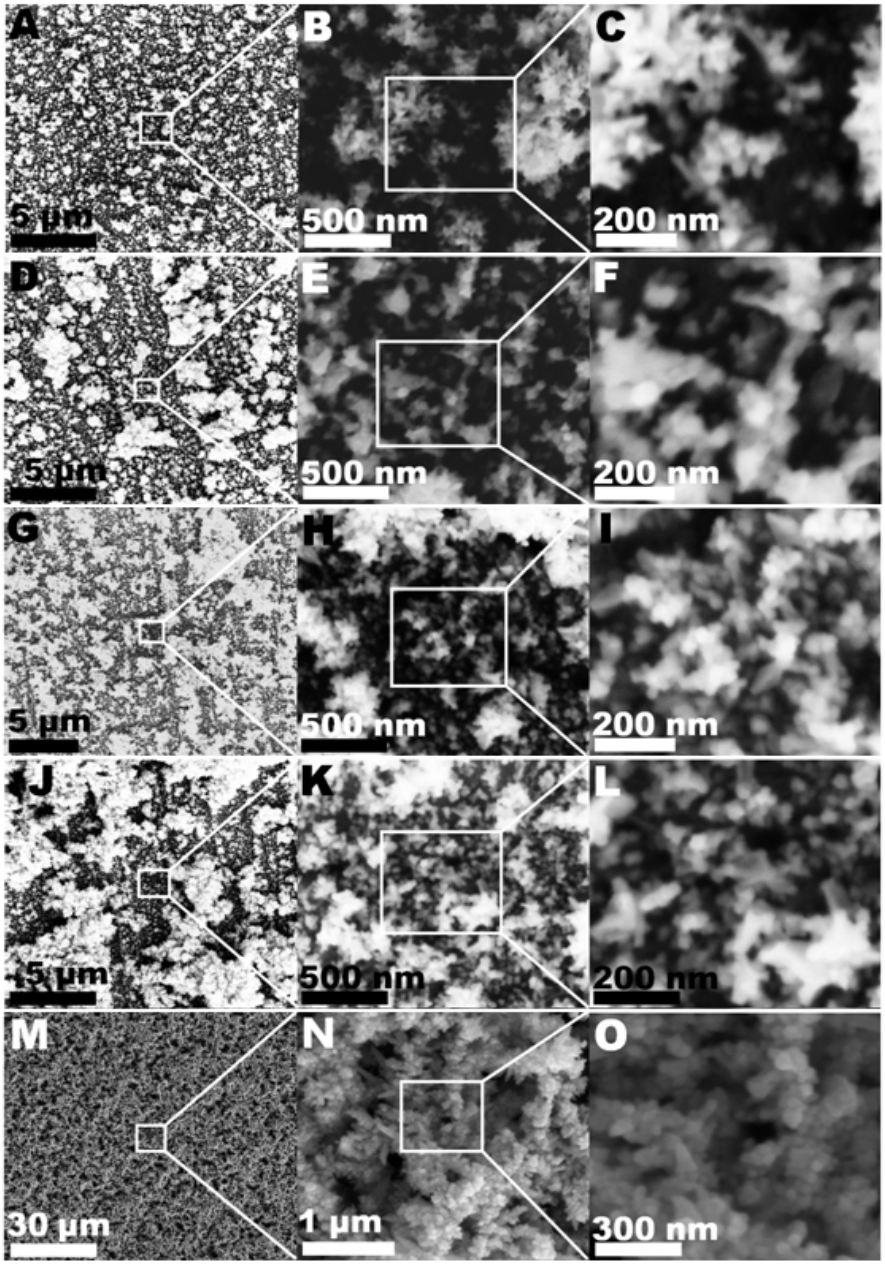

Figure 3. Top-view SEM images of 3D Cu films by field-stimulated assembly of Cu NPs under different conditions: (A-C) 10 mV for 4 min with an average current of ～27 mA; (D-F) 10 mV for 8 min with an average current of ～27 mA; (G-I) 100 mV for 4 min with an average current of ～45 mA; (J-L) 1000 mV for 4 min with an average current of ～54 mA; and (M-O) 2000 mV for 8 min with an average current of ～75 mA.

Let us consider the film morphology deposited under specific conditions that were used most often in this study in greater details. A segmented Cu films made of

islands with a characteristic dimension of ～310 nm were formed on the Cu foils under a potential of 10 mV and current of ～27 mA for 4 min (**Figure 3A-C**). In turn, each of these islands, was a dendritic structure made of grains <50 nm in size. Increasing the deposition time to 8 min, resulted in the increase of the protruding out-of-plane islands (**Figure 3D-F**). The average pores and interstitial spaces of these Cu NP films were ～50 nm (**Figure 3G-I**). By increasing the applied potential and reaction time, the dendritic islands grew larger resulting in the formation of additional sub-pores (**Figure 3J-O**). All of the pores were less than 5 μm with an average pore size of ～200 nm in diameter (**Figure 3M-O**). Lower-magnification SEM analysis using a 3D Cu film revealed a uniform surface structure (**Figure S3**), and the thickness of 3D Cu film was determined to be ～10 μm (**Figure 4A**). Even inside the Cu film kept the porous dendritic structure (**Figure 4B**), which was composed of small crystal grains of <100 nm (**Figure 4C**).

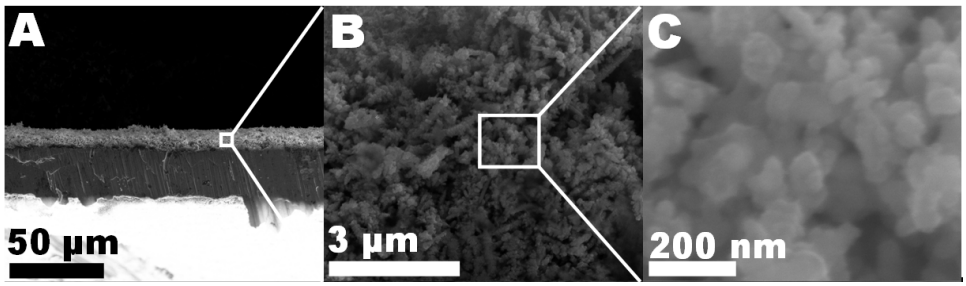

Figure 4. Cross-sectional SEM images of 3D Cu films by field-stimulated assembly of Cu NPs (corresponded to Figure 2M-O) under 2000 mV for 8 min with an average current of ～75 mA.

TEM was further used to investigate the structure of NP-assembled Cu films made under 2000 mV (～75 mA) for 8 min (**Figure 5** and **Figure S4**). As expected we observed dendrites with a branch length ranging from several tens of nanometer to

several micrometers (**Figure 3A** and **Figure S4A-C**), which is consistent with the SEM images (**Figure 2S-U**). Further examination at higher magnification showed that the dendrites were structured as hierarchical assemblies.

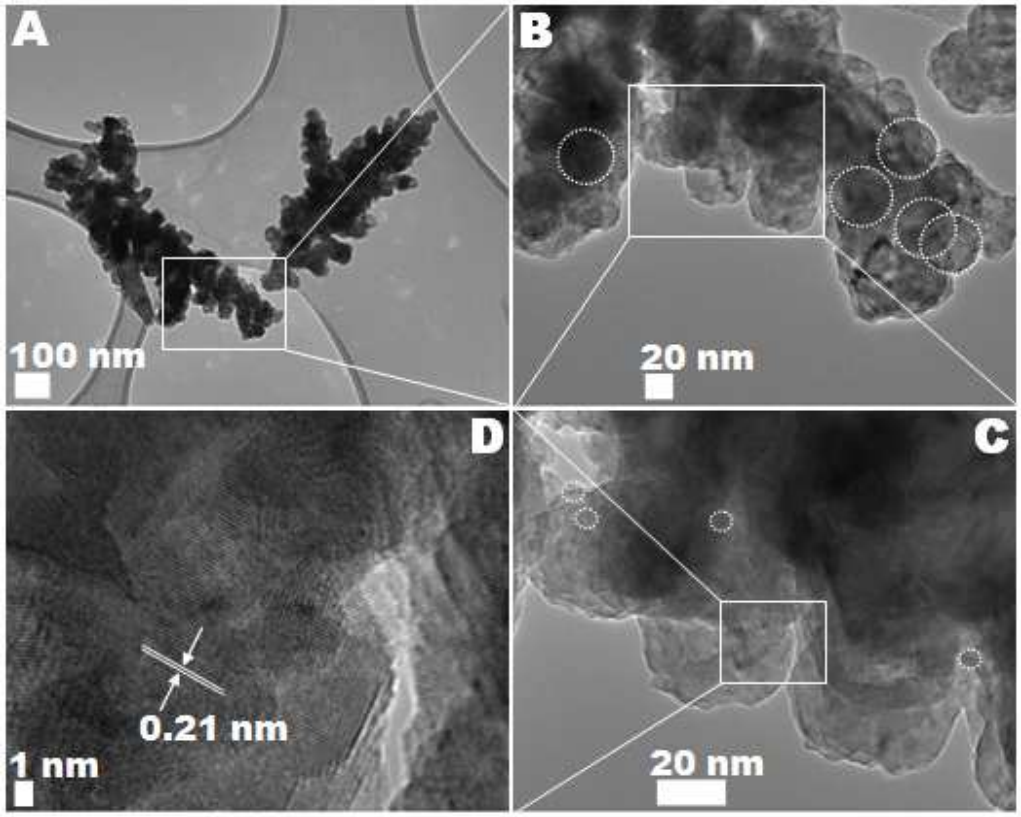

Figure 5. (A-D) TEM images of pieces of 3D Cu film obtained by field-stimulated assembly of Cu NPs (potential 2000 mV, current 75 mA, time 8 min).

Their constitutive units were NP agglomerates with the size of 30-50 nm (**Figure 5B** and **Figure S4D**). They were composited of interconnected individual NPs with the size of 2-8 nm (**Figure 5C** and **Figure S4D-E**) that corresponded very well with the size of NPs observed for dispersions in **Figure 1**. Importantly, in these assemblies we did not observe any interparticle gaps that would be attributable to CTAB stabilizer. Expectations of insulating organic shells around NPs and related poor charge transport might have prevented earlier studies of such films for current

collectors or other components of batteries. Contrary, we observed distinct NP-to-NP bridging (**Figure 5C** and **Figure S4E**) with lattice-to-lattice connectivity (**Figure 5D** and **Figure S4F**). Such morphology of the interparticle interface is conducive to metallic charge transport in the prepared Cu film. As a verification of the conductive nature of the NP-NP bridges, the lattice spacing in the interfacial areas between the NPs was estimated to be 0.21 nm (**Figure 5D** and **Figure S4F**); it corresponded very well to the lattice planes (111) of FCC Cu. The spontaneous formation of NP-NP bridges was previously observed for semiconductor NPs[49,62], but it was not observed for metallic particles. This observations are essential for the successful integration of NP self-assembly phenomena in technology of electronic and energy storage devices.

2.3. Performance of Cu NP-based current collectors. Electro-deposited porous Cu films as current collectors have been proven to improve the cycle performance of LIBs.[20-21,23,42] Here, we evaluated the electrochemical performance of current collectors from field-stimulated NP-assembled 3D porous and flat Cu electrodes using graphite (**Figure S5**) as electroactive intercalation material in coin-type half cells (**Figure 6**, **Figure S6**, and **Table 1**). In the first two C-D voltage curves (**Figure 6A-B**), during the first discharge process, the voltage dropped rapidly and formed a plateau centered at ~0.5 V, corresponding to the electrolyte decomposition and the formation of a solid electrolyte interface (SEI) film on the graphite surface.[63] After the first plateau, the voltage gradually decreased and the second plateau appeared at ~0.1 V, corresponding to the lithium extraction from graphite.[64-65] In each

charging process, a long voltage plateau was observed at ~0.25 V, suggesting the formation of LiC_6.[63] The charge- and discharge capacity in the first cycle for the flat Cu electrode were 71.2 mAh g^{-1} and 129.7 mAh g^{-1}, respectively, with a irreversible capacity of 58.2 mAh g^{-1}, due to the formation of a SEI film. The NP-based Cu electrode exhibited a higher charge and discharge capacity in the first cycle of 106.0 mAh g^{-1} and 169.1 mAh g^{-1}, respectively. After the first discharge process, the SEI film covering on the graphite surface forms and as a result of that, the irreversible capacity of both flat and NP-based Cu electrodes decreased to 9.5 mAh g^{-1} in the second cycle. Also, the NP-based Cu electrode still exhibited a higher discharge capacity (149.5 mAh g^{-1}) than the flat Cu electrode (113.9 mAh g^{-1}) in the second cycle.

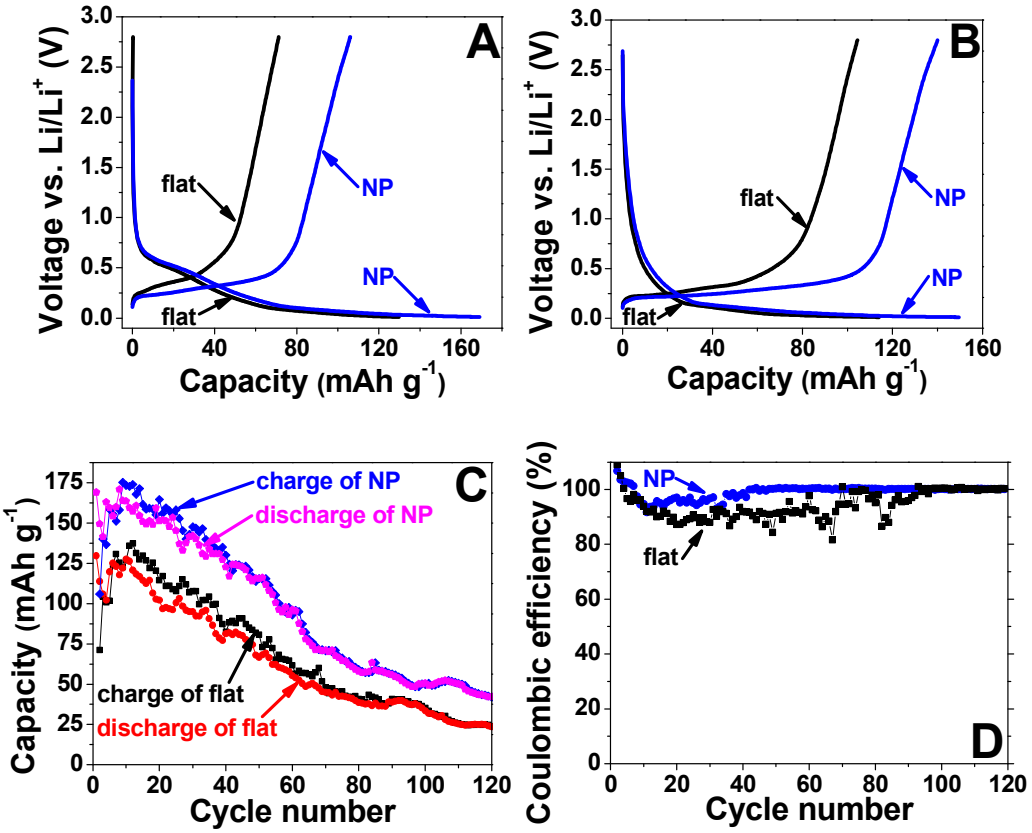

Figure 6. The (A) first and (B) second charge-discharge curves. (C) Dependence of cell capacity on the number of charge-discharge cycles, and (D) Coulombic efficiencies for flat and NP-based Cu half-cells at 0.25 C rate using 17.0 mg graphite as working material.

In the test evaluating the cycle performance (**Figure 6C**), flat Cu electrodes had a maximum discharge capacity of 129.7 mAh g^{-1}, while the NP-based Cu electrode showed a higher maximum capacity of 171.0 mAh g^{-1}. After 120 cycles, the NP-based Cu electrode preserved a discharge capacity of 42.4 mAh g^{-1}, which was almost twice of the flat Cu electrode (23.6 mAh g^{-1}). Additionally, the NP-based Cu electrode had higher Coulombic efficiencies than the flat Cu electrode (**Figure 6D**). Especially, after 40 C-D cycles, the NP-based Cu electrode maintained a Coulombic efficiency of nearly 100%. Note that the NP-based Cu electrodes showed higher capacities and retention values than the flat Cu electrodes upon various mass loadings (**Table 1**). Note that integration of carbon particles within the 3D topography of the field-assembled current collectors is suboptimal at the moment. The cross-sectional images of the electrodes in **Figure 4** and **S5** indicate that the deep penetration of fairly large carbon platelet-like particles from the slurry can be hindered and the data in **Figure 6** are likely to be greatly improved when a different electrode material or a better method of its deposition is utilized.

Table 1. Cycle performance of "flat" and 3D NP-based Cu current collectors

mass loading (mg)	electrode type	specific capacity (mAh g^{-1})		total capacity (μAh)		retention (%)
		Maximum	120^{th} cycle	maximum	120^{th} cycle	
17.0	flat	129.7	23.6	2204.9	401.2	18.2
	3D NPs	171.0	42.4	2872.8	712.3	24.8

11.5	flat	202.4	50.1	2307.4	571.1	24.8
	3D NPs	191.0	69.2	2215.6	802.7	36.2
7.0	flat	270.4	126.4	1892.8	884.8	46.7
	3D NPs	264.9	164.9	1827.8	1137. 8	62.2
3.0	flat	320.7	182.2	865.9	491.9	56.8
	3S NPs	292.0	242.0	934.4	774.4	82.9

The processes that can lead to capacity fade in lithium ion batteries include electrolyte decomposition, active material dissolution, phase changes in the electrode materials, and passive film formation over the electrode and current collector surfaces.[66] The high internal stress resulted from the lithium intercalation and deintercalation reactions lead to delamination of the working electrode materials from the flat current collectors.[65,67] These physical changes diminish the contact area between the working electrode materials and flat current collectors, which resulted in the low Coulombic efficiency and capacity degeneration.[3,5,67-69] However, the 3D out-of-plane structures assembled from NPs can not only increase the contact with electroactive materials but also relieve some internal stress from the volume change of electroactive materials,[4,70-71] therefore, the Coulombic efficiency and capacity of 3D Cu electrodes were greatly improved.[15]

We summarized the electrochemical parameters of our 3D porous electrodes field-assembled from NPs made with graphite as working electrode materials in **Table 2**. When compared with typical electrode materials such as Si, Sn-Co, Cu_6Sn_5, Sn, and Sn-Sb-Co, the total capacity value of our 3D porous electrodes (1138 μAh using 6.9 mg of graphite) was superior, even with a lower specific capacity. This was due to the greater amounts of graphite material prepared by a "slurry coating" method.

Table 2 Performance comparison of 3D Cu electrodes with other electrode materials.

electrode materials	weight (mg)	cycle number	C rate	specific capacity (mAh g^{-1})	total capacity (μAh)	reference
graphite	6.9	120	0.25	165	1138	our
	3.2	120	0.25	242	774	
Sn-Co	≤ 0.5	70	0.12	511	≤ 256	13
Si	≤ 2.62	63	0.05	750	≤ 1965	20
Sn	2.8	20	0.10	200	560	22
	1.2	20	0.10	460	552	
Cu_6Sn_5	≤ 1.6	40	1.00	250	≤ 400	23
Sn-Sb-Co	< 0.5	150	0.20	513	< 257	31
Cu_2O		120	< 0.10		1450	72
Sn	0.8	100	0.10	404	323	73
Fe_3O_4	≤ 0.23	100	2.16	< 1500	< 345	74
Si	0.173	100	0.10	1628	282	75

Note that graphite slurries used here can perform as both cathodes and anodes in LIBs depending on the design of the battery.

Understanding why the NP-based Cu electrodes exhibited improved electrochemical performance in comparison to flat Cu electrodes is essential. Impedance measurements allowed us to determine electrochemical kinetic parameters (**Figure 7A-C**). The proposed equivalent circuit for the half cell model (**Figure 7D**) was used to obtain the quantitative analysis according to previous studies.[76-77] $\boldsymbol{R_e}$ is the electrolyte resistance, $\boldsymbol{C_f}$ and $\boldsymbol{R_f}$ are the capacitance and resistance of the SEI film, respectively, $\boldsymbol{C_{dl}}$ and $\boldsymbol{R_{ct}}$ are the double-layer capacitance and charge-transfer resistance, respectively, and $\boldsymbol{Z_w}$ is the Warburg impedance, related to the lithium-diffusion process. Electrochemical kinetic parameters for NP-based and flat Cu electrodes with various mass loadings of graphite were summarized in **Table 3**.

For these mass loadings, the NP-based Cu electrodes showed lower R_f and R_{ct} values than flat Cu electrodes. The decrease of resistance from the flat Cu electrodes to their NP-based Cu counterparts should be ascribed to the thinner SEI formation and tighter attachment of electroactive intercalation materials on the 3D porous conductive filaments visible in Figures 4,5.[22] Moreover, the impedance plots of both flat and NP-based Cu electrodes after 50 and 100 cycles showed that the R_{ct} of flat Cu electrode increased greater with the C-D cycle than the NP-based Cu electrode (**Figure S7**). This point was further verified that the NP-based Cu electrode preserved good contact with the electroactive materials after long-term C-D cycles.

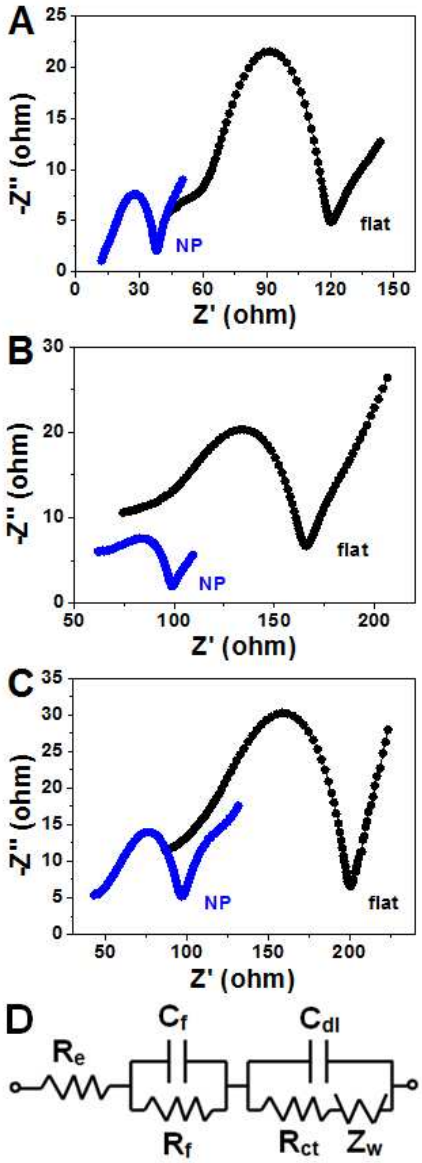

Figure 7. Impedance spectra of flat and NP-based Cu current collectors after 120 charge-discharge cycles at 0.25 C rate with (A) 7.0, (B) 11.5, (C) 17.0 mg graphite loading. (D) Equivalent circuit of half cell model.

To gain insight into the intercalation reaction between the graphite and lithium ions, we calculated exchange current densities (i_o) for traditional flat and 3D NP-based current collectors, according to an equation (1):[63,76-78]

$$i_o = \frac{RT}{nFR_{ct}} \qquad (1)$$

where R is the gas constant, T is the absolute temperature, n is the number of

transferred electrons, and ***F*** is the Faraday constant. When the weight of graphite was 17.0 mg, the i_o of the NP-based Cu electrode was calculated to be 7.4×10^{-4} A cm^{-2}, which was twice that of the flat Cu electrode (3.6×10^{-4} A cm^{-2}). Even when the graphite weight was decreased to approximately 11.5 and 7.0 mg, 3D Cu electrodes still showed higher i_o values than flat Cu electrodes. The higher electrochemical activities of NP-based Cu electrodes must stem from the 3D out-of-plane protrusions with large surface area, which effectively improved their physical and electrical contacts with electroactive materials and facilitated migration of lithium ions within the electrodes.

Table 3 Comparison of kinetic parameters for "flat" and 3D NP-based current collectors

graphite (mg)	electrode type	R_f (ohm)	R_{ct} (ohm)	i_o (A cm^{-2})
17.0	Flat	32.21	71.43	3.6×10^{-4}
	NP-based	16.33	34.60	7.4×10^{-4}
11.5	Flat	29.94	54.03	4.8×10^{-4}
	NP-based	15.39	19.38	1.3×10^{-3}
7.0	Flat	18.24	52.52	4.9×10^{-4}
	NP-based	6.08	17.49	1.5×10^{-3}

3. CONCLUSIONS

Well-dispersed ~3 nm Cu NPs synthesized in aqueous media enabled us to carry field-stimulated assembly to obtain a NP-based Cu films with high porosity. The efficient charge transport in the film was facilitated by the lattice-to-lattice connectivity between NPs and the lack of insulating gaps associated with CTAB protective coating. The use of NP dispersion enabled 30x reduction of current during the preparation of 3D conductive film. NP-based filed-assembled current collectors revealed considerably improved total capacity and other electrochemical parameters compared to the flat electrodes carrying the same amount of graphite. The 3D electrodes from field-assembled NPs also exhibited better cycle performance than the "flat" Cu electrodes, due to their tighter contact with working electrode material. Better mitigation of volume changes and acceleration of the diffusion of lithium ions may play a role as well. Further improvements are expected with tighter integration of the electroactive material (carbon or other) with the 3D electrodes assembled from NPs. The further study will focus on the application of higher-capacity anode materials, such as silicon, to improve the specific capacity in LIBs.

4. METHODS

4.1. Materials and chemicals. *L*-ascorbic acid, cetyltrimethylammonium bromide (CTAB), copper chloride dihydrate ($CuCl_2 \cdot 2H_2O$), acetone, acetic acid, and sulfuric acid were purchased from Sigma-Aldrich. Deionized water was obtained from a

Barnstead E-pure water purification system.

4.2. Synthesis of Cu NPs. A 25 mL aqueous solution containing 0.8 M *L*-ascorbic acid and 0.01 M CTAB and a 25 mL aqueous solution containing 0.06 M $CuCl_2 \cdot 2H_2O$ and 0.01 M CTAB were prepared, and then the two solutions above were mixed and heated at 45 ^oC for 42 hours under strong magnetic stirring. The resulting mixture turned from green/light brown to red, indicating the formation of Cu NPs.[53-54] The pure Cu NP solution with high dispersity was obtained by centrifugation at 10,000 rpm for three times (30 min each time), followed by dialysis for 1 hour to remove excessive *L*-ascorbic acid, CTAB, and copper chloride.

4.3. Field-stimulated assembly of Cu NPs. For the preparation of 3D porous Cu films, the copper foils were pretreated with dilute hydrochloric acid (7.4 wt%), acetone, and deionized water, respectively. A field-stimulated 3D porous Cu film was obtained using an Epsilon electrochemical workstation (Bioanalytical Systems, Inc.) under two electrode conditions, using a Pt wire as the anode and a Cu foil as the cathode. The distance between the two parallel electrodes was approximately 1 cm. The electrolyte was Cu NPs dispersed in a mixture of 0.4 M acetic acid and 2 mM CTAB solution. For Cu NP deposition on Cu foils, a chronoamperometry (CA) technique was applied under various potentials and time. As a control sample, electro-deposition using Cu^{2+} ions was performed under two electrode conditions, where two Cu foils were used as anode and cathode, respectively. The electrolyte was a mixture of 0.05 M $CuSO_4$, 3 M sulfuric acid, 0.2 M acetic acid, and 2 mM CTAB solution. CA was applied at a potential of 800 mV for 8 min. After the deposition

process, all of the samples were washed with ethanol and water sequentially several times, and were then dried under vacuum at 60 ^{o}C. The area densities of electro-deposited 3D Cu films were 1.25, 0.16, 0.20, 0.26, 0.30, and 0.40 mg cm^{-2}, respectively, by weighing completely scraped 3D Cu films as described in **Figure 2** (**A-F**), (**G-I**), (**J-L**), (**M-O**), (**P-R**) and (**S-X**).

4.4. Assembly of lithium ion battery half-cell models. To prepare the electrode using a "slurry coating" method, a mixture of graphite from MTI Corporation (size: 0.5-5 μm; fixed carbon: 99.9-99.99%) and polyvinylidene fluoride (PVDF, as a polymeric binder) with a weight ratio of 90:10 was dispersed and homogenized in N-methylpyrrolidone (NMP). The slurry was then pasted on the flat and 3D Cu electrodes and was dried under vacuum at 80 ^{o}C for 36 hours (**Figure S5**). For comparative evaluation of performance for flat versus 3D current collectors, the graphite loads of 17.0 and 16.8 mg, 11.4 and 11.6 mg, 7.0 and 6.9 mg, and 2.7 and 3.2 mg were pasted on the flat and NP-based Cu electrodes (1 cm × 1 cm) were labeled as 17.0, 11.5, 7.0, and 3.0 mg, respectively.

A two-electrode CR2032 coin cell was constructed with a Celgard LIB polyethylene separator from MTI Corporation. A lithium foil and a graphite-pasted Cu foil were used as the counter/reference electrode and working electrode, respectively. 1 M lithium hexafluorophosphate ($LiPF_6$) in a solution of 1:1 volume ratio of ethylene carbonate (EC) and dimethyl carbonate (DMC) was used as the electrolyte. The sandwich cell was assembled in a glove box filled with argon (oxygen content: < 3 ppm; moisture content: < 3 ppm).

4.5. Structural characterization. Transmission electron microscope (TEM) images were obtained using a JEOL 3011. The TEM specimens of Cu NPs were prepared by dripping a single drop of Cu NP aqueous solution onto a carbon-coated gold grid and then allowing the drop to dry in air. The average size of the Cu NPs was calculated by counting 754 particles from TEM images and was also measured by dynamic light scattering (DLS) (Zetasizer Nano-ZS, Malvern Instruments, U.K.). The 3D Cu films were scraped from Cu electrodes and then were dispersed in deionized water under an ultrasonication treatment of 10 seconds for TEM characterization. Scanning electron microscope (SEM) images were obtained using a FEI Nova 200 SEM.

4.6. Electrochemical characterization. The C-D cycle was conducted using a Maccor Series 4000 48-channel battery tester (Maccor, USA) in the voltage range of 0.01-2.8 V (vs. Li^+/Li) at 0.25 C rate. Electrochemical impedance spectroscopy (EIS) measurements were carried out using lithium foil as both counter and reference electrodes, and graphite-pasted Cu electrode as the working electrode. Before the EIS measurements, all the electrodes were discharged to 0.01 V and then left on open-circuit condition for one day to obtain equilibrium. As for the flat and NP-based Cu current collectors after 50 and 100 C-D cycles, the impedance spectra were obtained using a CHI660D electrochemical workstation (CH Instrument Inc., USA) by applying a sine wave with an amplitude of 5 mV over a frequency range from 100 k to 0.01 Hz. As for the current collectors after 120 C-D cycles, the impedance spectra were obtained using an Autolab PGSTAT302N Potentiostat/Galvanostat (Ecochemie, Netherlands) by applying a sine wave with an amplitude of 10 mV over a frequency

range from 100 k to 0.1 Hz. The impedance spectra were fitted to a proposed equivalent circuit using a code ZSimpWin (EChem Software Company, USA).

Supporting Information Available: TEM image and size distribution of Cu NPs by a DLS technology, SEM images of pretreated foil for the preparation of 3D Cu film, SEM and TEM images of 3D Cu film by field-stimulated of Cu NPs, SEM images of graphite mixed slurry on 3D Cu current collector after drying, cycle performance of various graphite loadings on flat and NP-based Cu electrodes at 0.25 C rate, and impedance spectra of flat and NP-based Cu current collectors with 7.0 mg graphite loading after 50 and 100 C-D cycles.

Acknowledgment. We thank the Electron Microscopy and Analysis Laboratory (EMAL) in University of Michigan for its assistance of electron microscopy. We also thank the Phoenix Memorial Laboratory in University of Michigan for the assembly and electrochemical tests of lithium ion coin cells. We are also greatly grateful to China Scholarship Council and Northwestern Polytechnical University for the scholarships to L. Liu. This project was supported by Samsung as a part of GRO program. This material is based upon work partially supported by the Center for Solar and Thermal Energy Conversion, an Energy Frontier Research Center funded by the U.S. Department of Energy, Office of Science, and Office of Basic Energy Sciences under Award Number #DE-SC0000957.

REFERENCES

1. Lou, X. W.; Deng, D.; Lee, J. Y.; Feng, J.; Archer, L. A. Self-Supported Formation of Needlelike Co_3O_4 Nanotubes and Their Application as Lithium-Ion Battery Electrodes. Advanced Materials **2008**, *20*, 258-262.
2. (a) Kang, K.; Meng, Y. S.; Breger, J.; Grey, C. P.; Ceder, G. Electrodes with high power and high capacity for rechargeable lithium batteries. Science **2006**, *311*, 977-980.
   (b) Tung S.O.; Ho, S.; Yang, M.; Zhang R.; Kotov, N. A.; A Dendrite-Suppressing Solid Ion Conductor From Aramid Nanofibers, Nature Comm, **2015**, *6*, 6152.
3. Zhang, S.; Jow, T. Study of poly (acrylonitrile-methyl methacrylate) as binder for graphite anode and $LiMn_2O_4$ cathode of Li-ion batteries. Journal of Power Sources **2002**, *109*, 422-426.
4. Xu, W.; Canfield, N. L.; Wang, D.; Xiao, J.; Nie, Z.; Li, X. S.; Bennett, W. D.; Bonham, C. C.; Zhang, J.-G. An approach to make macroporous metal sheets as current collectors for lithium-ion batteries. Journal of The Electrochemical Society **2010**, *157*, A765-A769.
5. Chen, L.; Xie, X.; Xie, J.; Wang, K.; Yang, J. Binder effect on cycling performance of silicon/carbon composite anodes for lithium ion batteries. Journal of Applied Electrochemistry **2006**, *36*, 1099-1104.
6. Magasinski, A.; Zdyrko, B.; Kovalenko, I.; Hertzberg, B.; Burtovyy, R.; Huebner, C. F.; Fuller, T. F.; Luzinov, I.; Yushin, G. Toward efficient binders for Li-ion battery Si-based anodes: Polyacrylic acid. ACS Applied Materials & Interfaces **2010**, *2*, 3004-3010.
7. Stournara, M.; Xiao, X.; Qi, Y.; Johari, P. S.; Lu, P.; Sheldon, B. W.; Gao, H.; Shenoy, V. B. Li segregation induces structure and strength changes at the amorphous Si/Cu interface. Nano Letters **2013**, *13*, 4759-4768.
8. Fan, X.-Y.; Zhuang, Q.-C.; Wei, G.-Z.; Huang, L.; Dong, Q.-F.; Sun, S.-G. One-step electrodeposition synthesis and electrochemical properties of Cu_6Sn_5 alloy anodes for lithium-ion batteries. Journal of Applied Electrochemistry **2009**, *39*, 1323-1330.
9. Beaulieu, L.; Eberman, K.; Turner, R.; Krause, L.; Dahn, J. Colossal reversible volume changes in lithium alloys. Electrochemical and Solid-State Letters **2001**, *4*, A137-A140.
10. Arbizzani, C.; Lazzari, M.; Mastragostino, M. Lithiation/delithiation performance of Cu_6Sn_5 with carbon paper as current collector. Journal of The Electrochemical Society **2005**, *152*, A289-A294.
11. Lee, J.-H.; Paik, U.; Hackley, V. A.; Choi, Y.-M. Effect of poly (acrylic acid) on adhesion strength and electrochemical performance of natural graphite negative electrode for lithium-ion batteries. Journal of Power Sources **2006**, *161*, 612-616.
12. Huang, L.; Zheng, X.-M.; Wu, Y.-S.; Xue, L.-J.; Ke, F.-S.; Wei, G.-Z.; Sun, S.-G. Electrodeposition and lithium storage performance of novel three-dimensional porous Fe-Sb-P amorphous alloy electrode. Electrochemistry Communications **2009**, *11*, 585-588.
13. Xue, L.-J.; Xu, Y.-F.; Huang, L.; Ke, F.-S.; He, Y.; Wang, Y.-X.; Wei, G.-Z.; Li, J.-T.; Sun, S.-G. Lithium storage performance and interfacial processes of three dimensional porous Sn–Co alloy electrodes for lithium-ion batteries. Electrochimica Acta **2011**, *56*, 5979-5987.
14. Yu, Y.; Chen, C. H.; Shui, J. L.; Xie, S. Nickel-Foam-Supported Reticular CoO-Li_2O Composite Anode Materials for Lithium Ion Batteries. Angewandte Chemie International Edition **2005**, *44*, 7085-7089.
15. Ji, H.; Zhang, L.; Pettes, M. T.; Li, H.; Chen, S.; Shi, L.; Piner, R.; Ruoff, R. S. Ultrathin

graphite foam: a three-dimensional conductive network for battery electrodes. Nano Letters **2012**, *12*, 2446-2451.

16. Arbizzani, C.; Beninati, S.; Lazzari, M.; Mastragostino, M. Carbon paper as three-dimensional conducting substrate for tin anodes in lithium-ion batteries. Journal of Power Sources **2005**, *141*, 149-155.
17. Arbizzani, C.; Beninati, S.; Lazzari, M.; Mastragostino, M. On the lithiation-delithiation of tin and tin-based intermetallic compounds on carbon paper current collector-substrate. Journal of Power Sources **2006**, *158*, 635-640.
18. Bruce, P. G.; Scrosati, B.; Tarascon, J. M. Nanomaterials for rechargeable lithium batteries. Angewandte Chemie International Edition **2008**, *47*, 2930-2946.
19. Guo, Y. G.; Hu, J. S.; Wan, L. J. Nanostructured materials for electrochemical energy conversion and storage devices. Advanced Materials **2008**, *20*, 2878-2887.
20. Jiang, T.; Zhang, S.; Qiu, X.; Zhu, W.; Chen, L. Preparation and characterization of silicon-based three-dimensional cellular anode for lithium ion battery. Electrochemistry Communications **2007**, *9*, 930-934.
21. Huang, L.; Wei, H.-B.; Ke, F.-S.; Fan, X.-Y.; Li, J.-T.; Sun, S.-G. Electrodeposition and lithium storage performance of three-dimensional porous reticular Sn-Ni alloy electrodes. Electrochimica Acta **2009**, *54*, 2693-2698.
22. Jiang, T.; Zhang, S.; Qiu, X.; Zhu, W.; Chen, L. Preparation and characterization of tin-based three-dimensional cellular anode for lithium ion battery. Journal of Power Sources **2007**, *166*, 503-508.
23. Shin, H. C.; Liu, M. Three-Dimensional Porous Copper-Tin Alloy Electrodes for Rechargeable Lithium Batteries. Advanced Functional Materials **2005**, *15*, 582-586.
24. Huang, X.; Tu, J.; Zeng, Z.; Xiang, J.; Zhao, X. Nickel Foam-Supported Porous NiO/Ag Film Electrode for Lithium-Ion Batteries. Journal of The Electrochemical Society **2008**, *155*, A438-A441.
25. Beattie, S.; Manolescu, D.; Blair, S. High-capacity lithium–air cathodes. Journal of The Electrochemical Society **2009**, *156*, A44-A47.
26. Cui, Y.; Wen, Z.; Liu, Y. A free-standing-type design for cathodes of rechargeable Li-O_2 batteries. Energy & Environmental Science **2011**, *4*, 4727-4734.
27. Grootenhuis, P.; Powell, R.; Tye, R. Thermal and electrical conductivity of porous metals made by powder metallurgy methods. Proceedings of the Physical Society. Section B **1952**, *65*, 502.
28. Zhang, E.; Wang, B. On the compressive behaviour of sintered porous coppers with low to medium porosities-Part I: Experimental study. International Journal of Mechanical Sciences **2005**, *47*, 744-756.
29. El-Hadek, M. A.; Kaytbay, S. Mechanical and physical characterization of copper foam. International Journal of Mechanics and Materials in Design **2008**, *4*, 63-69.
30. Hassoun, J.; Panero, S.; Simon, P.; Taberna, P. L.; Scrosati, B. High-Rate, Long-Life Ni-Sn Nanostructured Electrodes for Lithium-Ion Batteries. Advanced Materials **2007**, *19*, 1632-1635.
31. Ke, F.-S.; Huang, L.; Solomon, B. C.; Wei, G.-Z.; Xue, L.-J.; Zhang, B.; Li, J.-T.; Zhou, X.-D.; Sun, S.-G. Three-dimensional nanoarchitecture of Sn-Sb-Co alloy as an anode of lithium-ion batteries with excellent lithium storage performance. Journal of Materials Chemistry **2012**, *22*,

17511-17517.

32. Taberna, P.-L.; Mitra, S.; Poizot, P.; Simon, P.; Tarascon, J.-M. High rate capabilities Fe_3O_4-based Cu nano-architectured electrodes for lithium-ion battery applications. Nature Materials **2006**, *5*, 567-573.
33. Hyun, S.; Murakami, K.; Nakajima, H. Anisotropic mechanical properties of porous copper fabricated by unidirectional solidification. Materials Science and Engineering: A **2001**, *299*, 241-248.
34. Park, J.; Hyun, S.; Suzuki, S.; Nakajima, H. Effect of transference velocity and hydrogen pressure on porosity and pore morphology of lotus-type porous copper fabricated by a continuous casting technique. Acta Materialia **2007**, *55*, 5646-5654.
35. Zhao, Y.; Fung, T.; Zhang, L.; Zhang, F. Lost carbonate sintering process for manufacturing metal foams. Scripta Materialia **2005**, *52*, 295-298.
36. Li, Y.; Jia, W.-Z.; Song, Y.-Y.; Xia, X.-H. Superhydrophobicity of 3D porous copper films prepared using the hydrogen bubble dynamic template. Chemistry of Materials **2007**, *19*, 5758-5764.
37. Shin, H.-C.; Liu, M. Copper foam structures with highly porous nanostructured walls. Chemistry of Materials **2004**, *16*, 5460-5464.
38. Nikolić, N. D.; Branković, G.; Popov, K. I. Optimization of electrolytic process of formation of open and porous copper electrodes by the pulsating current (PC) regime. Materials Chemistry and Physics **2011**, *125*, 587-594.
39. Hayes, J.; Hodge, A.; Biener, J.; Hamza, A.; Sieradzki, K. Monolithic nanoporous copper by dealloying Mn-Cu. Journal of Materials Research **2006**, *21*, 2611-2616.
40. Qi, Z.; Zhao, C.; Wang, X.; Lin, J.; Shao, W.; Zhang, Z.; Bian, X. Formation and Characterization of Monolithic Nanoporous Copper by Chemical Dealloying of Al-Cu Alloys. The Journal of Physical Chemistry C **2009**, *113*, 6694-6698.
41. Lee, K. T.; Lytle, J. C.; Ergang, N. S.; Oh, S. M.; Stein, A. Synthesis and Rate Performance of Monolithic Macroporous Carbon Electrodes for Lithium-Ion Secondary Batteries. Advanced Functional Materials **2005**, *15*, 547-556.
42. Fan, X.-Y.; Ke, F.-S.; Wei, G.-Z.; Huang, L.; Sun, S.-G. Sn-Co alloy anode using porous Cu as current collector for lithium ion battery. Journal of Alloys and Compounds **2009**, *476*, 70-73.
43. Meng, Q.-B.; Fu, C.-H.; Einaga, Y.; Gu, Z.-Z.; Fujishima, A.; Sato, O. Assembly of highly ordered three-dimensional porous structure with nanocrystalline TiO_2 semiconductors. Chemistry of Materials **2002**, *14*, 83-88.
44. Ba, J.; Polleux, J.; Antonietti, M.; Niederberger, M. Non-aqueous Synthesis of Tin Oxide Nanocrystals and Their Assembly into Ordered Porous Mesostructures. Advanced Materials **2005**, *17*, 2509-2512.
45. Zhu, G.; Qiu, S.; Gao, F.; Li, D.; Li, Y.; Wang, R.; Gao, B.; Li, B.; Guo, Y.; Xu, R. Template-assisted self-assembly of macro-micro bifunctional porous materials. Journal of Materials Chemistry **2001**, *11*, 1687-1693.
46. Yuan, C.; Zhang, X.; Su, L.; Gao, B.; Shen, L. Facile synthesis and self-assembly of hierarchical porous NiO nano/micro spherical superstructures for high performance supercapacitors. Journal of Materials Chemistry **2009**, *19*, 5772-5777.
47. Sawai, K.; Iwakoshi, Y.; Ohzuku, T. Carbon materials for lithium-ion (shuttlecock) cells. Solid State Ionics **1994**, *69*, 273-283.

48. Yoo, E.; Kim, J.; Hosono, E.; Zhou, H.-S.; Kudo, T.; Honma, I. Large reversible Li storage of graphene nanosheet families for use in rechargeable lithium ion batteries. Nano Letters **2008**, *8*, 2277-2282.

49. Kim, J.-Y.; Kotov, N. A. Charge transport dilemma of solution-processed nanomaterials. Chemistry of Materials **2013**, *26*, 134-152.

50. Jung, S.H.; Chen, C.; Cha, S-H.; Yeom, B.; Bahng, J.H.; Srivastava, S.; Zhu, J.; Yang, M.; Liu, S; Kotov, N.A. Spontaneous Self-Organization Enables Dielectrophoresis of Small Nanoparticles and Formation of Photoconductive Microbridges. J. Am. Chem. Soc. 2011, *133* (28), 10688–10691.

51. Kim, Y.; Zhu, J.; Yeom, B.; Di Prima, M.; Su, X.; Kim, J.-G.; Yoo, S. J.; Uher, C.; Kotov, N. A. Stretchable nanoparticle conductors with self-organized conductive pathways. Nature **2013**, *500*, 59-63.

52. Kobayashi, Y.; Ishida, S.; Ihara, K.; Yasuda, Y.; Morita, T.; Yamada, S. Synthesis of metallic copper nanoparticles coated with polypyrrole. Colloid and Polymer Science **2009**, *287*, 877-880.

53. Yu, W.; Xie, H.; Chen, L.; Li, Y.; Zhang, C. Synthesis and characterization of monodispersed copper colloids in polar solvents. Nanoscale Research Letters **2009**, *4*, 465-470.

54. Wang, Y.; Asefa, T. Poly (allylamine)-stabilized colloidal copper nanoparticles: synthesis, morphology, and their surface-enhanced Raman scattering properties. Langmuir **2010**, *26*, 7469-7474.

55. Shi, M.; Kwon, H. S.; Peng, Z.; Elder, A.; Yang, H. Effects of surface chemistry on the generation of reactive oxygen species by copper nanoparticles. ACS Nano **2012**, *6*, 2157-2164.

56. Li, X.; Zhu, D.; Wang, X. Evaluation on dispersion behavior of the aqueous copper nano-suspensions. Journal of Colloid and Interface Science **2007**, *310*, 456-463.

57. Yanase, A.; Komiyama, H. In situ observation of oxidation and reduction of small supported copper particles using optical absorption and X-ray diffraction. Surface Science **1991**, *248*, 11-19.

58. Jian-Guang, Y.; Yuang-Lin, Z.; Okamoto, T.; Ichino, R.; Okido, M. A new method for preparing hydrophobic nano-copper powders. Journal of Materials Science **2007**, *42*, 7638-7642.

59. Kim, J. H.; Germer, T. A.; Mulholland, G. W.; Ehrman, S. H. Size-Monodisperse Metal Nanoparticles via Hydrogen-Free Spray Pyrolysis. Advanced Materials **2002**, *14*, 518-521.

60. Wu, C.; Mosher, B. P.; Zeng, T. One-step green route to narrowly dispersed copper nanocrystals. Journal of Nanoparticle Research **2006**, *8*, 965-969.

61. (a) Kanninen, P.; Johans, C.; Merta, J.; Kontturi, K. Influence of ligand structure on the stability and oxidation of copper nanoparticles. Journal of Colloid and Interface Science **2008**, *318*, 88-95.

(b) Kobayashi, Y.; Sakuraba, T. Silica-coating of metallic copper nanoparticles in aqueous solution. Colloids and Surfaces A: Physicochemical and Engineering Aspects **2008**, *317*, 756-759

62. (a). Tang, Z.; Kotov, N.A.; Giersig, M. Spontaneous Organization of Single CdTe Nanoparticles into Luminescent Nanowires. Science **2002**, *297*(5579), 237–240; (b) Querejeta-Fernández, A.; Hernández-Garrido, J.C.; Yang, H.; Zhou, Y.; Green, P.F.; Varela, A.;

Parras, M.; Calvino-Gámez, J.J; González-Calbet, J.M.; Kotov, N.A. Unknown Aspects of Self-Assembly of PbS Microscale Superstructures. ACS Nano **2012**, *6*(5), 3800–3812.

63. Guo, P.; Song, H.; Chen, X. Electrochemical performance of graphene nanosheets as anode material for lithium-ion batteries. Electrochemistry Communications **2009**, *11*, 1320-1324.
64. Yang, S.; Huo, J.; Song, H.; Chen, X. A comparative study of electrochemical properties of two kinds of carbon nanotubes as anode materials for lithium ion batteries. Electrochimica Acta **2008**, *53*, 2238-2244.
65. Cao, Y.; Xiao, L.; Ai, X.; Yang, H. Surface-modified graphite as an improved intercalating anode for lithium-ion batteries. Electrochemical and Solid-State Letters **2003**, *6*, A30-A33.
66. Arora, P.; White, R. E.; Doyle, M. Capacity fade mechanisms and side reactions in lithium-ion batteries. Journal of The Electrochemical Society **1998**, *145*, 3647-3667.
67. Guoping, W.; Bolan, Z.; Min, Y.; Xiaoluo, X.; Meizheng, Q.; Zuolong, Y. A modified graphite anode with high initial efficiency and excellent cycle life expectation. Solid State Ionics **2005**, *176*, 905-909.
68. Ramadass, P.; Haran, B.; White, R.; Popov, B. N. Mathematical modeling of the capacity fade of Li-ion cells. Journal of Power Sources **2003**, *123*, 230-240.
69. Wang, C.; Appleby, A. J.; Little, F. E. Charge-discharge stability of graphite anodes for lithium-ion batteries. Journal of Electroanalytical Chemistry **2001**, *497*, 33-46.
70. Takamura, T.; Uehara, M.; Suzuki, J.; Sekine, K.; Tamura, K. High capacity and long cycle life silicon anode for Li-ion battery. Journal of Power Sources **2006**, *158*, 1401-1404.
71. Kim, Y.-L.; Sun, Y.-K.; Lee, S.-M. Enhanced electrochemical performance of silicon-based anode material by using current collector with modified surface morphology. Electrochimica Acta **2008**, *53*, 4500-4504.
72. Liu, D.; Yang, Z.; Wang, P.; Li, F.; Wang, D.; He, D. Preparation of 3D nanoporous copper-supported cuprous oxide for high-performance lithium ion battery anodes. Nanoscale **2013**, *5*, 1917-1921.
73. Xue, L.; Fu, Z.; Yao, Y.; Huang, T.; Yu, A. Three-dimensional porous Sn-Cu alloy anode for lithium-ion batteries. Electrochimica Acta **2010**, *55*, 7310-7314.
74. Wu, H.; Du, N.; Wang, J.; Zhang, H.; Yang, D. Three-dimensionally porous Fe_3O_4 as high-performance anode materials for lithium-ion batteries. Journal of Power Sources **2014**, *246*, 198-203.
75. YoubáKim, D.; WookáKim, D. Electrodeposited 3D porous silicon/copper films with excellent stability and high rate performance for lithium-ion batteries. Journal of Materials Chemistry A **2014**, *2*, 2478-2481.
76. Yang, S.; Song, H.; Chen, X. Electrochemical performance of expanded mesocarbon microbeads as anode material for lithium-ion batteries. Electrochemistry Communications **2006**, *8*, 137-142.
77. Chang, Y. C.; Jong, J. H.; Fey, G. T. K. Kinetic characterization of the electrochemical intercalation of lithium ions into graphite electrodes. Journal of The Electrochemical Society **2000**, *147*, 2033-2038.
78. Wang, G.; Bradhurst, D.; Dou, S.; Liu, H. Spinel $Li[Li_{1/3}Ti_{5/3}]O_4$ as an anode material for lithium ion batteries. Journal of Power Sources **1999**, *83*, 156-161.